Seismic Tomography using Graph Theoretical Ray Tracing

Youngseuk Keehm[1], Chang-Eob Baag[1], and Jung Mo Lee[2]

[1] Dept. of Geological Sciences, Seoul National University,
San 56-1, Shillim-dong, Kwanak-ku, Seoul, 151-742, Korea

[2] Dept. of Geology, Kyungpook National University,
Taegu, 702-701, Korea

(Manuscript received 10 October, 1997)

Abstract

Seismic tomography using the graph theoretical method of ray tracing is performed in two synthetic data sets with laterally varying velocity structures. The straight-ray tomography shows so poor results in imaging the laterally varying velocity structure that the ray-traced tomographic techniques should be used. Conventional ray tracing methods have serious drawbacks, i.e. problems of convergence and local minima, when they are applied to seismic tomography. The graph theretical method finds good approximated raypaths in rapidly varying media even in shadow zones, where shooting methods meet with convergence problems. The graph theoretical method ensures the globally minimal traveltime raypath while bending methods often cause local minima problems. Especially, the graph theoretical method is efficient in case that many sources and receivers exist, since it can find the traveltimes and corresponding raypaths to all receivers from a specific source at one time. Moreover, the algorithm of graph theoretical method is easily applicable to the ray tracing in anisotropic media, and even to the three dimensional case. Among the row-active inversion techniques, the conjugate gradient (CG) method is used because of fast convergence and high efficiency. The iterative sequence of the ray tracing by the graph theoretical method and the inversion by the CG method is an efficient and robust algorithm for seismic tomography in laterally varying velocity structures.

1. Introduction

Seismic tomography is a useful tool to estimate subsurface seismic velocity structures. It provides a high resolution image of the earth using the traveltimes given by the seismic wave fields passed through the earth. Radon (1917) suggested the basic idea of tomography that the propagation of seismic energy through a medium can be described by an integral or a sum of the properties of the medium over the raypath. He showed that the properties of the medium can be calculated, if a complete set of sums or integrals is measured. This idea has been applied to many fields including radio astronomy, material testing, medical imaging, civil engineering, and geophysical explorations. Aki *et al.* (1977) performed the three dimensional inversion for seismic structures of lithosphere. Recent examples using the seismic tomography include Bregman *et al.* (1989), Lees and Crosson (1989), Lines and LaFehr (1989), Chen *et al.* (1990), Woodward (1992), and Tura *et al.* (1992).

In seismic tomography, the medium to be imaged is divided into a number of cells, each of which has the velocity distribution. For the efficiency of the numerical calculations, we assumed homogeneous and isotropic rectangular cells. The traveltimes are not linearly related to the slowness, since the raypaths depend upon the unknown velocity structure. When the dependence of the raypaths on velocity structure can be ignored i.e., only weakly non-linear cases, the straight-ray can be used to obtain similar results (Dines and Lytle, 1979; Lines and LaFehr, 1989), and it has been used frequently in both synthetic and real data inversion studies (McMechan, 1983; Scales, 1987). However, some studies show the straight-ray tomography has shown poor results in rapidly varying media (Ivansson, 1985; Bregman *et al.*, 1989). Then, the iterative sequence of ray-tracing and linear inversion is necessary to good tomograms of rapidly varying media. Some conventional methods for ray tracing, however, have serious drawbacks when applied to tomography. Therefore the graph theoretical method (Moser, 1991) based on network theory is used, which is fast and robust against inhomogeneity of media.

In geophysical application, sources and receivers are rarely placed on all sides of the imaging region, and this gives some subregions of very poor ray coverage. Moreover, seismic tomography cannot sometimes find the true velocity of regions of apparently good ray coverage, if most raypaths are oriented to a specific direction. McMechan (1983) and Bregman *et al.* (1989) showed that the structures perpendicular to the raypaths have very poor resolution. Thus, both spatial coverage and angular coverage are important and must be considered carefully for good results. The source-receiver geometry is an important factor of seismic tomography. The source-receiver geometry includes VSP (vertical seismic profiling), RVSP (reversed vertical seismic profiling), and XSP (crosshole seismic profiling). Many studies of seismic tomography have used XSP, since the local earth structure is usually subhorizontal. RVSP produces seismic sections similar to those of the conventional VSP, and the RVSP data can be collected more rapidly and economically (Chen *et al.* 1990). The combination of XSP and RVSP has advantages in ray coverage and data collection economy, since it is easily set by adding the surface receivers to the crosshole scheme. We use this combination scheme and ideal scheme where sources and receivers exist on all sides of the imaging region.

The iterative sequence of ray tracing and inversion is adopted. We use the graph theoretical method of ray tracing and the CG inversion method, since the CG and the SIRT(simultaneously iterative reconstruction technique) show similar results but the CG converges faster than the SIRT.

2. Graphical Method of Ray Tracing

The forward modeling step associated with ray tracing in the current estimate of seismic velocity structure, is the most expensive step in any traveltime inversion or tomographic algorithm. It is therefore essential to choose the appropriate ray tracing method to produce optimal results for the particular model representation. Two conventional methods, shooting and bending methods, have serious drawbacks. Shooting method causes the convergence problem when used in laterally varying media, and it cannot find diffracted raypaths and raypaths in shadow zones. Bending method often reaches the local minima instead of finding the globally minimal traveltimes of first arrivals.

To overcome these drawbacks, the graph theoretical method is used in this study. The graph theoretical method is derived from network theory, and it is applied to many branches of science and technology; city planning, electronic circuit design, and seismic ray tracing. It is based on discrete nature; it represents continuous objects or properties as discrete ones. In many cases, this approximation is fairly accurate and efficient. One example is road map, where the network consists of cities and connections between them. And then we want to find the shortest route from one city to another to minimize the traveltime. In seismic ray tracing, shortest paths mean the raypaths which have minimal traveltimes. One important property of seismic ray is given by Fermat's principle; a wave propagates along a raypath for which the traveltime is minimum. The construction of a raypath connecting two points can be based on this principle. The graph theoretical method provides an alternative use of Fermat's principle.

The part of the earth can be represented by a network consisting of points or nodes (Fig. 1). Each node is connected with finite number of nodes named *forward stars*, and has traveltime $t(i)$. Δt_{ij} which denotes the traveltime between the i-th node and the j-th node, is expressed as,

$$\Delta t_{ij} = \int_{node\ i}^{node\ j} p(x, y, z)\ dr. \tag{1}$$

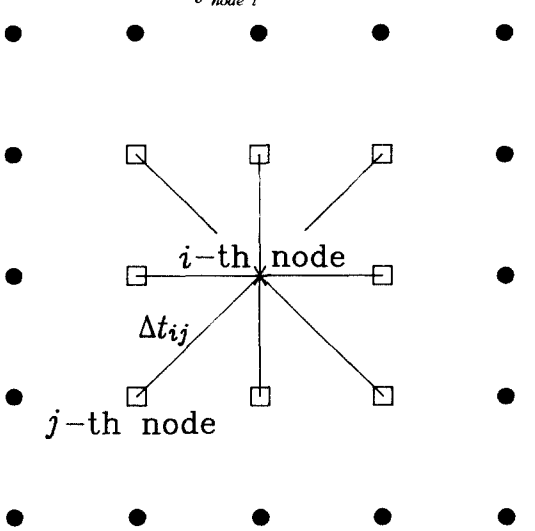

Fig. 1. Schematic illustration of network organization: Each node is connected with neighboring eight nodes named forward star nodes. Δt_{ij} denotes the traveltime between the i-th node and the j-th node.

Therefore a ray travels from one node to another via the connection. The connections are called arcs. As on a road map, the connections between two nodes have lengths, the length is to be understood as a weight of connection. Take for an example, in seismic ray tracing, it is the traveltime of a seismic wave between the two nodes. In other application of electrical network, the weight can be the electrical resistance. For efficiency of calculations, a regular distribution of the nodes and straight connections have been proposed. Nakanishi and Yamaguchi(1986) used the network that eight nodes are distributed regularly on the boundaries of rectangular cells in which the propagation velocity of seismic wave is constant. In this study, the rectangular grid is used, and the cells in each of which the seismic velocity is constant and isotropic, are bounded by neighboring four nodes. The accuracy of traveltimes and corresponding raypaths by the graph theoretical method is dependent not only upon the total number of nodes but upon the number of forward stars. These factors are known as space dicretization and angle dicretization. The angular structure of the forward star set is carefully determined, and the set with 176 forward stars is used in this study.

We define a graph $G(N,A)$, with a set N containing n nodes and an arc set A. The arc set A is usually incomplete set, since all two nodes are not connected. A network $(G,\Delta T)$ is a graph with a weighting function ΔT that assigns a real number to each arc. ΔT can be represented by a square matrix, Δt_{ij} . For ray tracing purpose, ΔT is symmetric by virtue of reciprocity, $\Delta t_{ij} = \Delta t_{ji}$, and non-negative, $\Delta t_{ij} > 0$. And, $\Delta t_{ij} = \Delta t_{ji} = \infty$ denotes the case that the nodes i and j are not connected. The forward star set of the node i, $FS(i)$, is the set of nodes connected with i. Then, a path $P(ID,r)$ has a sequence of nodes which are connected successively each other.

$$P(ID,r) = (s, i_1, i_2, i_3, \ldots\ldots, r), \tag{2}$$

where s denotes the source node, r the receiver node and ID the identity of the path. The traveltime $t(r)$ along the path is defined as the sum of weights of the connections along the path,

$$t(r) = \sum_{k=s}^{r} \Delta t_{k,k+1}. \tag{3}$$

There are many paths connecting two nodes s and r. Next, we find the shortest path that has a minimal traveltime among these raypaths with an algorithm, a so-called shortest path tree. The shortest path tree structure enables the shortest paths to be described by using an array pointer, $prec(i)$, the preceding node of i on the shortest path from s to r. A shortest path can be extracted from this array by repeating $\{j = prec(i);\ i = j\}$ until $i = s$. The shortest traveltime from the source point s follows Bellman's equations:

$$t(i) = min\ [\ t(j)+\Delta t_{ij}\ ]\quad (i \neq j)\qquad i,j \in N, \tag{4}$$

and its initial condition is

$$t(s)=0. \tag{5}$$

The nodes are divided into two sets, a set P of nodes with known minimal traveltimes and a set Q of nodes with not yet known minimal traveltimes. Initially P is empty, and $Q=N$. The traveltimes of all nodes are

infinite except for source node, $t(s)=0$. The preceding history of the source node, $prec(s)$ is its own. Then we can calculate Δt_{sj} for $j \in FS(s)$, and apply the Bellman's equation to this calculation of traveltimes. The traveltimes and preceding histories of these forward star nodes are updated, since their initial values are infinite. The traveltime of source node, $t(s)$ is certainly minimal traveltime, so it can be transferred to P. In next step, there are all nodes except for the source node in the set Q. We find the node with minimal traveltime among nodes in the set Q, then the node can be a source node in the next step. We can also calculate the forward stars of this node and update the traveltimes and preceding histories by the Bellman's equation. It is now possible to repeat the nonlinear recursion for all nodes in N, until no traveltime is updated more. The shortest paths from one node to all other nodes are then calculated although not all information may be useful. These procedures are known as the Dijkstra's algorithm (Moser, 1991), and are summarized as;

(1) Initialization

$Q=N$, $t(i)=\infty$ for all $i \in N$

$P=\varnothing$, $t(s)=0$

(2) Selection

Find $i \in Q$ with minimal traveltime $t(i)$

Searching Forward Stars of the node i

(3) Updating

$t(j) = min \{ t(j), t(i)+ \Delta t_{ij} \}$ for all $j \in [FS(i) \cap Q]$

transfer i from Q to P

(4) Iteration Check

if $P=N$ stop

else goto (2).

Typical raypaths in the laterally varying medium are shown in Fig. 2 drawn by the graphical method. The network used in this model consists of 31×31 nodes, and the number of the forward stars is 176. Diffraction and refraction at the velocity discontinuities are well represented in Fig. 2. The raypaths can be more smooth and realistic, if the dense grid is used.

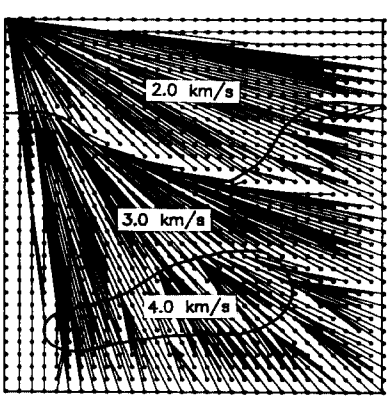

Fig. 2. Raypaths using the graph theoretical method with the network of 31x31 nodes in the laterally varying velocity structure; The seismic velocities of three regions are presented.

The constrained graph theoretical method can be applied to anisotropic cases. The algorithm of the graph theoretical method makes it easy to calculate the raypaths in anisotropic media; i.e. the forward star set from a specific node has angular characteristics of seismic rays, and if the anisotropy is given a function of the angle, we easily formulate the shortest path algorithm with anisotropy. Bakus (1965) presented the emperical equation of anisotropy as;

$$\rho a^2 = A + B\cos 2\psi + C\sin 2\psi + D\cos 4\psi + E\sin 4\psi, \quad (6)$$

where ρ is the density of the medium, a the P-wave velocity, and ψ the orientation of anisotropy. The raypaths in the isotropic media and in the media with an anisotropic region are illustrated in the velocity structure (Fig. 3). The dashed lines are raypaths in the isotropic case, and the solid lines are in the anisotropic case in which the transversely isotropic region with dark gray color exists. The fast velocity direction is denoted by longer bar in the cross symbol. The ratio of the fast velocity to the slow velocity is 1.2 in this model. The raypaths through the anisotropic region are distorted to the fast velocity direction.

The advantages of the graph theoretical method are; First, all shortest paths of one source are constructed simultaneously. There are many receivers for one source in seismic profiling, this method saves computation time a lot. Second, it needs no special differential equation for its algorithm. Though it seems to ignore the differential equations even Snell's law, it gives a direct, practical and accurate results of ray tracing. Third, this method, robust in presence of velocity discontinuities, gives well-approximated raypaths in rapidly varying media. Fourth, the graph theoreical method can find the distorted raypaths in anisotropic media, with small constraints of the standard algorithm. Last, It is easily applicable to three dimensional case with the same algorithm of two dimensional case.

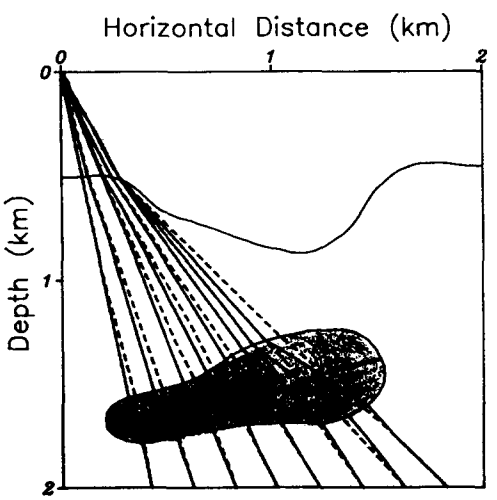

Fig. 3. Comparison of the raypaths in isotropic (dotted lines) and anisotropic (solid lines) cases : The region with dark gray color has transverse anisotropy. The longer bar of the cross symbol indicates the fast direction of the seismic velocity. The fast to the slow velocity ratio is 1.2.

3. Inversion Methods

The tomographic problem may be stated as "from projections measured outside of an object, find the interior distribution of the object's property". A projection is the sum of an object's parameters along a given path. A sum or integral of this type is known as a Radon transform (RT) which is closely related to the Fourier transform (FT). In many applications, projection data are interpreted using the Fourier transform theory or numerical inversion techniques. The RT is also known as a slant stack and is equivalent to the τ-p transform in the exploration seismology. Two alternative methods of inverse radon transform (IRT) are the filtered back projection (FBP) and the circular harmonic decomposition (CHD). These methods are developed for a continuous medium with full coverage. The series expansion techniques of the IRT are widely used in many applications. These techniques solve the seismic tomographic problems by row-action methods such as the algebraic reconstruction technique (ART), the SIRT, or the CG algorithm (Hestenes *et al.*, 1952). In this study, the CG method is used in order to get merit of its fast convergence,

In the series expansion methods, the forward modeling problem results in the matrix equation,

$$\mathbf{b} = \mathbf{A}\mathbf{x}, \tag{7}$$

where the column matrix $\mathbf{b}$ represents predicted data function, the column matrix $\mathbf{x}$ represents the estimated model function, and the $N \times M$ matrix $\mathbf{A}$ represents the ray segments.
The anomaly form obtained from the equation (7) is

$$\Delta\mathbf{b} = \mathbf{A}\Delta\mathbf{x}. \tag{8}$$

In order to get a proper from in the CG method, the equation (8) is applied by the transpose matrix of $\mathbf{A}$ as follows,

$$\mathbf{A}^T\Delta\mathbf{b} = \mathbf{A}^T\mathbf{A}\Delta\mathbf{x} \tag{9}$$

which describes the critical points of $\| \Delta\mathbf{b}-\mathbf{A}\Delta\mathbf{x} \|^2$. The matrix $\mathbf{A}^T\mathbf{A}$ is square, symmetric and non-negative. Equation (9) can completely characterize the least-square solutions of equation (8). If the matrix $\mathbf{A}$ has at least as many rows as columns and is full of rank, the least-square solution is unique and can be directly obtained by equation (8). On the other hand, if $\mathbf{A}$ is underdetermined or rank-deficient, the least-square solution is not unique. In this case we use the equation (9) for good convergence to the true value. The convergence of the CG method usually depends upon the initial guess. Hestenes (1975) showed that if the initial guess is taken to be zero, the CG algorithm converges to the minimum norm, least-square solution.

We suppose that $\mathbf{A}$ is an $N \times M$ matrix. Applying the CG algorithm to the inverse problem yields the following generalization: Choose the initial guess $\mathbf{x}^{(0)}$, put $\mathbf{s}^{(0)}=\mathbf{b}-\mathbf{A}\mathbf{x}^{(0)}$, $\mathbf{p}^{(0)}=\mathbf{r}^{(0)}=\mathbf{A}^T(\mathbf{b}-\mathbf{A}\mathbf{x}^{(0)})$, $\mathbf{q}^{(0)}=\mathbf{A}\mathbf{p}^{(0)}$. Then using the inner product notation, $(\mathbf{x},\mathbf{x})=\mathbf{x}^T\mathbf{x}=\mathbf{x}\cdot\mathbf{x}$,

$$\alpha^{(k+1)} = (\mathbf{r}^{(k)},\mathbf{r}^{(k)})/(\mathbf{q}^{(k)},\mathbf{q}^{(k)}), \tag{10-a}$$

$$\mathbf{x}^{(k+1)} = \mathbf{x}^{(k)}+\alpha^{(k+1)}\mathbf{p}^{(k)}, \tag{10-b}$$

$$\mathbf{s}^{(k+1)} = \mathbf{s}^{(k)}-\alpha^{(k+1)}\mathbf{q}^{(k)}, \tag{10-c}$$

$$\mathbf{r}^{(k+1)} = \mathbf{A}^T\mathbf{s}^{(k+1)}, \tag{10-d}$$

$$\beta^{(k+1)} = (\mathbf{r}^{(k+1)}, \mathbf{r}^{(k+1)})/(\mathbf{r}^{(k)},\mathbf{r}^{(k)}), \tag{10-e}$$

$$\mathbf{p}^{(k+1)} = \mathbf{r}^{(k)}+\beta^{(k+1)}\mathbf{p}^{(k)}, \tag{10-f}$$

$$\mathbf{q}^{(k+1)} = \mathbf{A}\mathbf{p}^{(k+1)}. \tag{10-g}$$

Note that the equation (10) avoids explicit calculation of $\mathbf{A}^T\mathbf{A}$. The idea is to calculate the residual $\mathbf{b}-\mathbf{A}\mathbf{x}$, then multiply by $\mathbf{A}^T$ rather than subtracting $\mathbf{A}^T\mathbf{A}\mathbf{x}$ from $\mathbf{A}^T\mathbf{b}$. As seen from equation (10), the CG algorithm consists of a few simple vector operations.

Simple synthetic calculations using the CG inversion method are performed without ray tracing process. The model structure is divided by 10×10 cells. Each cell has either of two different velocities, 1.0 km/sec or 2.0 km/sec. The velocity structure of this model is given in Fig. 4(a). Fig. 4(b) shows the initial guess of velocity distribution for the inversion process which has a constant value 1.5 km/sec at every cell. Two source-receiver configurations are used in this model in order to determine the dependence of inversion processes on the ray geometry. They are denoted by the configurations (A) and (B), respectively. The geometry of configuration (A) is the combination of RVSP and XSP (Fig. 4(c)). Fig. 4(d) shows the inversion result computed by the CG method after 30 iterations. In the lower part of the model the images of the vertical structures are rather poor, while the horizontal structures are well imaged. We can recall the fact that the structures oriented perpendicular to the raypaths result in poor resolution. Configuration (B) is an ideal case so that sources and receivers are located at all sides of boundary (Fig. 4(e)). All regions in the model structure have good coverage of ray path. Fig. 4(f) shows a clear image obtained by inversion.

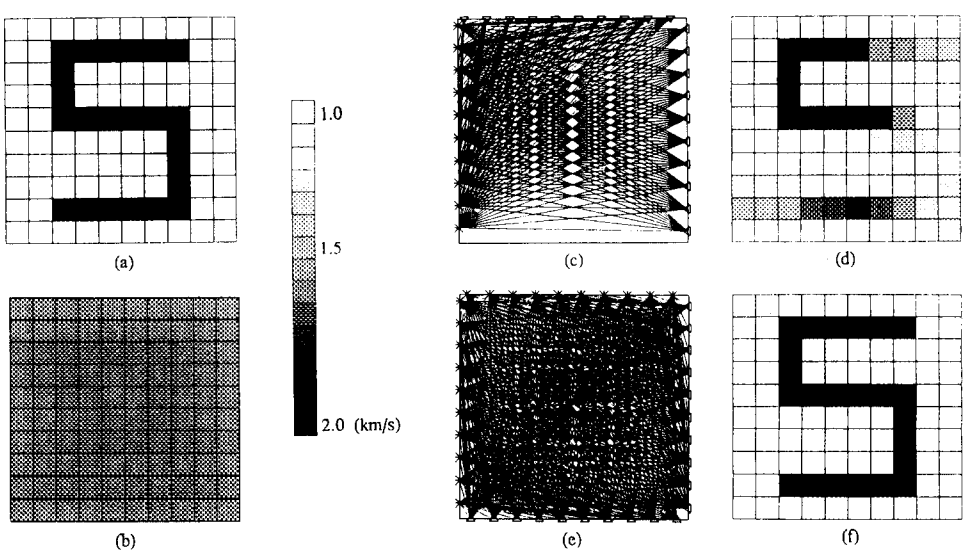

Fig. 4. Straight ray tomography using two source-receiver configurations: (a) presents the original velocity model used synthesizing traveltimes, (b) presents initial guess in inversion, (c) presents the practical source-receiver configuration named "configuration (A)" which consists of XSP and RVSP, (d) presents the tomogram using configuration (A), (e) presents the ideal source-receiver configuration named "configuration (B)" where sources and receivers at all sides of the boundary, and (f) presents the tomogram using the configuration (B).

4. Modeling and Discussion

Two synthetic models are used for the seismic tomographic inversion with the CG method and the graph theoretical method. These models are physically unrealistic since the data sets are noise-free. Each model consists of 30×30 inversion cells, and the network for the shortest path algorithms is composed of 121×121 nodes. Two source-receiver configurations illustrated in Fig. 4 are used

At each inversion step, the CG minimizes the residual $\mathbf{r} = |\mathbf{b}-\mathbf{Ax}|$ and updates the velocities from previous calculated velocities, until the residual is sufficiently small. If the ray segments matrix **A** is fully ranked, the calculated velocity model converges to the true model. Otherwise, the non-uniqueness problem occurs, i.e. the calculated model may converge to other local minima. Especially, this problem is so serious at earlier sequences. Thus, proper constraints of the iteration are needed; at earlier step, the iteration is limited to a small number, otherwise to the contrary.

The velocity structure of an oil-trap model is illustrated in Fig. 5(a), and the wavefronts created by the source at the upper-left corner is also shown in Fig. 5(b). This shows the distortion of the circular wavefronts at the velocity discontinuities. In Fig. 5(a), the upper part of the anticline may satisfy the oil-trap conditions. We can say that the part with the seismic velocity of 2.0 km/sec contains gas, and the part of 2.5 km/sec is an oil-trapped layer. The initial guess of the velocity distribution for the inversion is put as a constant, 3.0 km/sec, at every cell. The tomogram obtained by configuration (A) is given in Fig. 6(a), and that by configuration (B) in Fig. 6(b). The differences of the tomogram obtained by the practical source-receiver geometry of configuration (A) compared with those by the ideal configuration (B) are as follows;

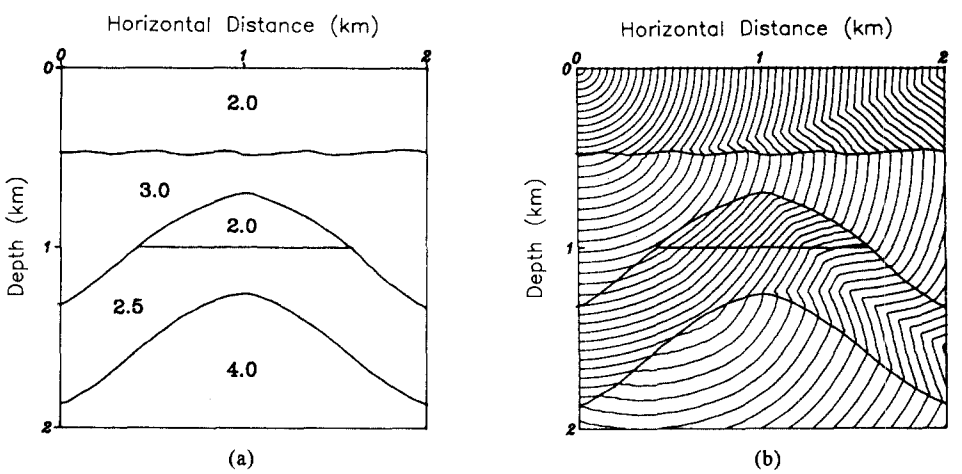

Fig. 5. Velocity structure of the oil-trap model and wavefronts propagated from a source; (a) presents a velocity structure of the oil-trap model where numbers denote seismic velocities, and (b) presents the wavefronts propagated from the source located at the upper left corner.

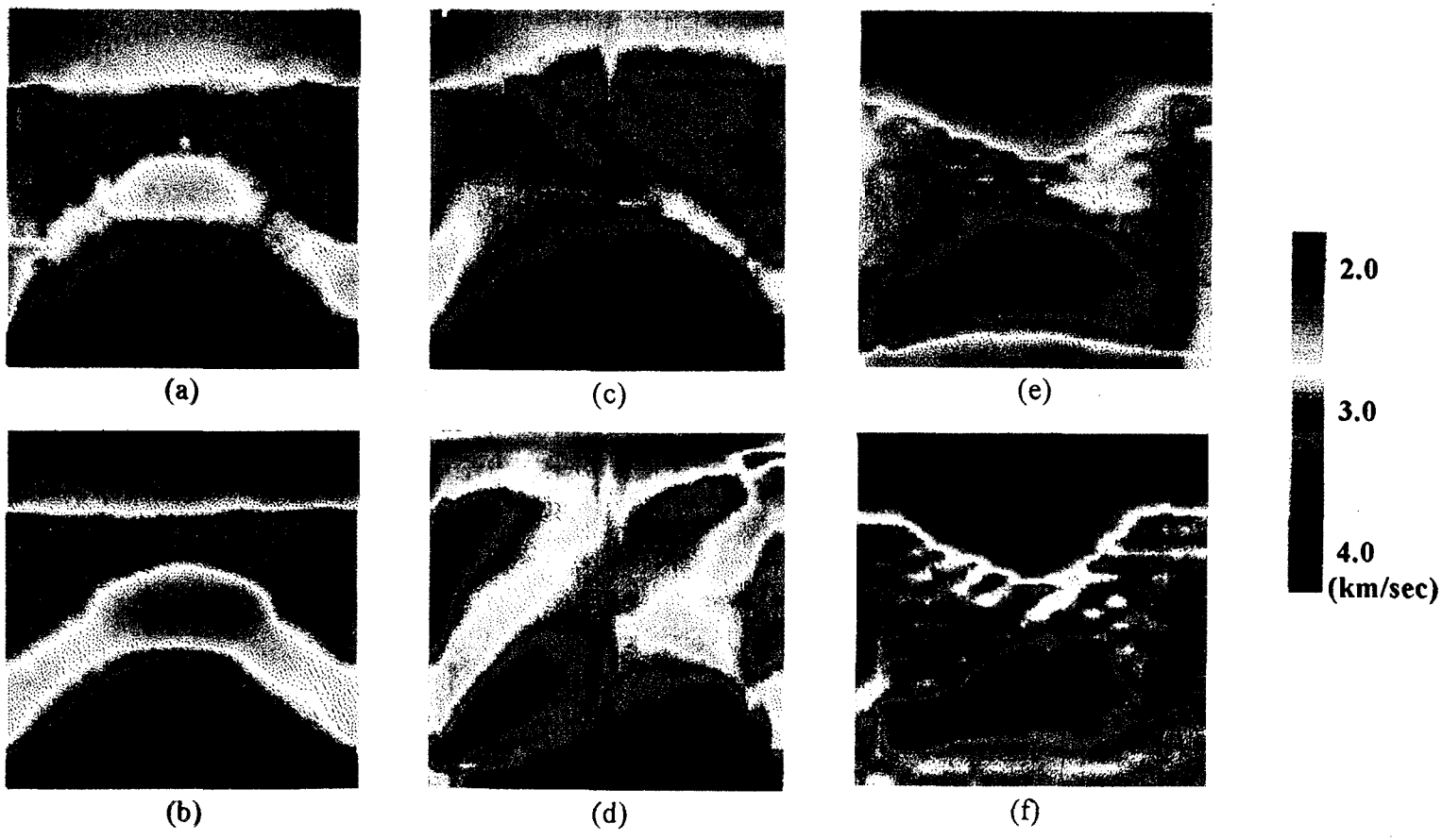

Fig. 6. Ray-traced tomography implemented by the graph theoretical method and the CG inversion method: (a) presents the ray-traced tomogram of the oil-trap model using configuration (A) of Fig. 4(c), (b) presents the ray-traced tomogram of the oil-trap model using configuration (B) of Fig. 4(e), (c) presents the straight ray tomogram of the oil-trap model using configuration (A), (d) presents the straight ray tomogram of the oil-trap model using configuration (B), (e) presents the ray-traced tomogram of the ore-body model of Fig. 3 using configuration (A), and (f) presents the ray-traced tomogram of the ore-body model using configuration (B).

(1) The structure of the velocity distribution is not clearly distinct. The boundaries of the velocity discontinuities are smooth rather than sharp. Especially, the low velocity zone is imaged poorly, since the first arrivals will not pass through this zone.

(2) The spatial high frequency noise is shown in Fig. 6(a). This fluctuation of the velocity field comes from a low coverage effect caused by excessive iteration of the inversion step. Thus, the determination of this optimal iteration number is important.

(3) The erroneous velocity anomaly can be found along the line from the left bottom to the right top (Fig. 6(a)), in spite of the better coverage than any other region. The cells near this line show exaggerated velocities. The left-lower part shows lower value, and the upper-right part shows higher value than the true one. From this effects, we can infer that the coverage difference has a considerable effect on the tomograms. If we have some parts that have larger coverage differences, the velocities of these parts may be overestimated.

Next, the straight-ray tomographic technique is also applied to imaging this model. The tomograms obtained by configuration (A) are shown in Fig. 6(c), and those by configuration (B) in Fig. 6(d). These tomograms are too poor to guess the true velocity structure. Oddly, the tomograms obtained by configuration (B) are more distorted than those by configuration (A), though configuration (B) has better coverage than configuration (A). The good coverage means the strong constraint for the convergence. However, this strong constraint by configuration (B) distorts the tomograms more seriously.

The ore-body model which was shown in Fig. 2, is also tomographically imaged. The tomograms obtained by configuration (A) is given in Fig. 6(e), and by configuration (B) in Fig. 6(f). Characteristics of these results are so similar to those in the previous model. The fluctuation of the velocity field can be seen in the medium with 3.0 km/sec of velocity due to the excessive iterations. More iterations in an inversion step produce the fluctuation of the velocity field. However they also give the distinct boundaries of the velocity discontinuities. Near the lower boundary of the model the true velocities of the cells are all 3.0 km/sec. However, the calculated velocities are lower than that in Fig. 6(e), since the first arrivals mostly pass through the high velocity region with 4.0 km/sec of velocity.

5. Conclusions

The graph theoretical method is very robust in seismic tomography, and it gives good approximations of globally minimal traveltimes and corresponding raypaths even in complicated velocity structure. It computes traveltimes and raypaths of all nodes at the same time. This is inefficient in the case of only one source-receiver pair, but it is very efficient in case that many source-receiver pairs are available. It can also find the raypaths in shadow zones. The convergence problems in shooting methods and the local minima problems in bending methods can be avoided using the graph theoretical method. It gives good approximate raypaths in the presence of velocity discontinuities. In addition, it gives a versatile tool for the ray tracings in anisotropic media.

In applications of seismic tomography, the geometry of sources and receivers mainly affects the tomogram of the expected region. The expected region must have not only good spatial coverage but also good angular coverage of raypaths. Moreover, the distribution of the coverage should be smooth, since the velocities calculated by tomographic techniques may be overestimated by the coverage differences. Seismic tomography using graph theoretical method and well-prepared source-receiver geometry gives good tomograms of the earth structure efficiently.

Acknowledgement

This study was partly supported by the academic research fund of Ministry of Education, Republic of Korea (BSRI-96-5406 and BSRI-96-5421).

References

Aki, K., Christoffersson, A., and Huseby, E. S., Determination of three dimensional seismic structure of the lithosphere, *J. Geophy. Res., 82,* 277-296, 1977.

Backus, M., Possible forms of seismic anisotropy in uppermost mantle under oceans, *J. Geophys. Res., 70.,* 3429-3439, 1965.

Bregman, N. D., Bailey, R. C., and Chapman, C. H., Crosshole seismic tomography, *Geophysics, 54,* 200-215, 1989.

Chen, S. T., Zimmerman, L. J., and Tugnait, J. K., Surface imaging using reversed vertical seismic profiling and crosshole tomographic methods, *Geophysics, 55,* 1478-1487, 1990.

Dines, K. and Lytle, J., Computerized geophysical tomography, *Proc. IEEE, 67,* 1065-1073, 1979.

Hestenes, M., 1975, Pseudoinverse and conjugate gradients, *Communications, Assn. Comp. Math., 18,* 40-43, 1975.

Hestenes, M. and Stiefel, E., Methods of conjugate gradients for solving linear systems, *Nat. Bur. Standards J. Res., 49,* 409-436, 1952.

Ivansson, S., A study of methods for tomographic velocity estimation in the presence of low-velocity zones, *Geophysics, 50,* 969-988, 1985.

Lees, J. M. and Crosson, R. S., Tomographic inversion for three-dimensional velocity structure at Mount St. Helens using earthquake data, *J. Geophy. Res., 94,* 5716-5728, 1989.

Lines, L. R. and LaFehr, E. D., Tomographic modeling of a cross-borehole data set, *Geophysics, 54,* 1249-1257, 1989.

McMechan, G. A., Seismic tomography in boreholes, *Geophys. J. R. astr. Soc., 74,* 601-612, 1983.

Moser, T. J., Shortest path calculation of seismic ray, *Geophysics, 56,* 59-67, 1991.

Nakanishi, I. and Yamaguchi, E., A numerical experiments on nonlinear image reconstruction from first arrival times for two dimensional island arc structure, *J. Phys. Earth, 34,* 195-201, 1986.

Radon, J., Über die Bestimmung von Funktionen durch ihre Integralwerte langs gewisser mannigfaltigkeiten, *Ber. Verh. Sachs. Akad, Wiss., 69,* 262-267, 1917

Scales, J. A., Tomographic inversion via the conjugate gradient method, *Geophysics, 52,* 179-185, 1987.

Tura, M. A. C., Johnson, L. R., Majer, E. L., and Peterson, J. E., Application of diffraction tomography to fracture detection, *Geophysics, 57,* 245-257, 1992.

Woodward M. J., Wave-equation tomography, *Geophysics, 57,* 15-26, 1992.